Article

Not peer-reviewed version

Measurement of the Effective Refractive Index of Suspensions Containing 5 µm Diameter Spherical Polystyrene Microparticles by Surface Plasmon Resonance and Scattering

Osvaldo Rodríguez-Quiroz *, Donato Luna-Moreno *, Araceli Sánchez-Álvarez, Gabriela Elizabeth Quintanilla-Villanueva, Oscar Javier Silva-Hernández, Melissa Marlene Rodríguez-Delgado, Juan Francisco Villarreal-Chiu

Posted Date: 10 June 2025

doi: 10.20944/preprints202506.0719.v1

Keywords: effective refractive index; particle; polystyrene; scattering; surface plasmon resonance; thin film

 doi:10.20944/preprints202506.0719.v1

Article

Measurement of the Effective Refractive Index of Suspensions Containing 5 μm Diameter Spherical Polystyrene Microparticles by Surface Plasmon Resonance and Scattering

Osvaldo Rodríguez-Quiroz [1,*], Donato Luna-Moreno [1,*], Araceli Sánchez-Álvarez [2], Gabriela Elizabeth Quintanilla-Villanueva [1], Oscar J. Silva-Hernández [1], Melissa Marlene Rodríguez-Delgado [3,4] and Juan Francisco Villarreal-Chiu [3,4]

[1] Centro de Investigaciones en Óptica A.C., Loma del Bosque 115, Colonia Lomas del Campestre, León Guanajuato, C.P. 37150, México

[2] Electromecánica Industrial, Universidad Tecnológica de León, Blvd. Universidad Tecnológica 225, Col. San Carlos, León 37670, Guanajuato, México

[3] Facultad de Ciencias Químicas, Universidad Autónoma de Nuevo León, Av. Universidad S/N Ciudad Universitaria, San Nicolás de los Garza 66455, Nuevo León, México

[4] Centro de Investigación en Biotecnología y Nanotecnología (CIByN), Facultad de Ciencias Químicas, Universidad Autónoma de Nuevo León, Parque de Investigación e Innovación Tecnológica, Km. 10 Autopista al Aeropuerto Internacional Mariano Escobedo, Apodaca 66629, Nuevo León, México

* Correspondence: osvaldo.rodriguez@cio.mx, dluna@cio.mx

Abstract: Microplastics (MP) have been found not only in the environment but also in living beings, including humans. As an initial step in MP detection, a method is proposed to measure the effective refractive index of a solution containing 5 μm diameter spherical polystyrene particles (SPSP) in distilled water, based on surface plasmon resonance (SPR) technique and Mie scattering theory. The reflectances of the samples are obtained with their resonance angles and depths that must be normalized and adjusted according to the reference of the air and the distilled water, to subsequently find its effective refraction index corresponding to the Mie scattering theory. The system has an optical sensor with a Kretschmann-Raether configuration, consisting of a semicircular prism, a thin gold film, and a cell for solutions samples with different concentrations (0.00, 0.20, 0.05, 0.50 and 1.00 %). The experimental result provided a good linear fit with an R^2=0.986, a sensitivity of 7.4526 $\times \mathbf{10^{-5}}$ RIU/%, LOD=0.001% and LOQ=0.0035%. The optomechatronic system and the applications developed for the SPR-Scattering theory allowed us to measure the effective refractive index and concentration for solutions with 5 μm diameter SPSP in distilled water.

Keywords: effective refractive index; particle; polystyrene; scattering; surface plasmon resonance; thin film

1. Introduction

Plastics are used in the manufacture of various products such as clothing, tires, cosmetics, paints, bags, rope, and netting. Plastics, made from a specific type of polymer, are lightweight, flexible, corrosion resistant, dielectric, thermal insulators, insoluble in water, most are not biodegradable, have the potential to absorb, release and transport chemicals, and gradually decompose by erosion or fragmentation through biological, chemical, and physical processes until they become solid microplastic (MP) particles with a size of 1 μm to 5 mm [1], or nanoplastics with a size of 1 nm to 1 μ [2].

In the analysis of plastic particles, it is desirable to know the shape, size, concentration, refractive index (RI), and effective refractive index of the sample (colloid or suspension). Tuoriniemi J. et al. [3] determined the mean diameters (d_{part}: 100, 300, and 460 nm) and number concentrations (ρ) of

 doi:10.20944/preprints202506.0719.v1

polystyrene (PS) particles by fitting coherent scattering theory (CST) to the effective refractive index (n_{eff}) measured by SPR for a series of dilutions. R. Márquez-Islas et al. [4] obtained the refractive index, size (radii of ~25 nm), and concentration of non-absorbing spherical nanoparticles in a colloid, using a mathematical method and measurements with the Abbe refractometer and with dynamic light scattering (DLS).

R.C. Thompson et al.[5] collected and quantified microplastic debris on beaches, estuarine and subtidal sediments, where nine polymers were identified : acrylic, alkyd, poly (ethylene: propylene), polyamide (nylon), polyester, polyethylene, polymethacrylate, polypropylene, and polyvinyl alcohol ; and demonstrated in small aquariums, that species would ingest microplastics within a few days. Microplastic debris is found throughout the natural environment, as it is transported through air and water, and has been detected in food, beverages, terrestrial animals, birds, and fish, with emerging evidence of negative effects [6]. A study of water distribution networks across Britain, from the treatment plant to the customer's tap, detected mainly polyamide (PA), polyethylene terephthalate (PET), polypropylene (PP), and polystyrene (PS), among 19 types of polymer particles, for sizes greater than 25 μm diameter [7].

Other research provides the presence, distribution, and potential ecological risks of MPs in terrestrial ecosystems [8], in water and aquatic systems [9], and ecotoxicological effects on aquatic organisms [10]. But MPs have not only been found in the environment; they have also been found in the human body, including blood. MPs are absorbed by the human body and transported through the bloodstream. In a study of 20 healthy volunteers, blood concentrations ranged from 1.84–4.65 μg/mL, with an average length of 7–3000 μm and an average width of 5–800 μm, and with 24 polymer types, with an abundance of polyethylene (32%), ethylene propylene diene (14%), and ethylene-vinyl-acetate/alcohol (12%), whose presence poses the risk of potential detrimental effects, such as vascular inflammation, accumulation in major organs, and alterations in immune response, hemostasis, and thrombosis [11]. The MPs have been found in food products like table salt, shellfish, fish, processed foods like honey, milk, sugar, sardines, sprats, dried fish, and tea bags[12]. Different studies have been carried out to assess the effects of the ingestion of MPs: Sapkale et al evaluated the oxidative damage caused by microplastics with size from in 8–100 μm in the ram's horn snail *Indoplanorbis exustus,* and found that the lethal concentration 50 (LC_{50}) was calculated to be 872 mg L^{-1} (or 0.087% w/v) after 96 h of exposure [13]. In another study, Berber evaluated the genotoxicity of polystyrene microplastic in the aquatic species *Daphnia magna,* calculating an LC_{50} of 808.97 μg mL^{-1} (or 0.08 % w/v) [14]. The common techniques used to determine one or more characteristics for nanoparticle detection are electron microscopy (EM) [3], spectroscopy, dynamic light scattering (DLS)[3,4] , and to detect microparticles, there are microspectroscopy, Fourier Transform Infrared (FTIR) [5,7,15], and Raman[16]. Therefore, it is important to establish regulations for industries that produce plastic, implement corrective measures for pollution, investigate the effects on living beings, and develop methods to detect and analyze nanoplastics and microplastic particles.

In this investigation, it is important to estimate the thickness of the thin gold film adhered to the prism surface by means of the theoretical experimental adjustment of the SPR curves[17]. The surface plasmon resonance technique[18–21] is employed to obtain the reflectance and resonance angle when the suspensions are placed in a cell prism. To determine the effective refractive index and the percentage of the fill fraction f (hereafter concentration) that corresponds to each reflectance, the scattering theory [22]and the Mie scattering theory[23] are applied. To simulate reflectance and calculate the effective refractive index of colloids (nanoparticles in distilled water) and suspensions (microparticles in distilled water), the formulas of coherent scattering theory [24,25] and the van der Hulst model [26] are used, respectively. In the experiments, we used a portable optomechatronic system and applications developed in LabVIEW and MATLAB [27], where the optical sensor (semicircular prism, thin gold film, and cell for samples) was placed in a Kretschmann-Raether configuration. Suspensions of 5 μm diameter SPSP in distilled water are prepared with different concentrations (0.00, 0.02, 0.05, 0.50, and 1.00 %). Each suspension is then scanned by the system to obtain its reflectance, which is normalized and adjusted to the reference point of the distilled water

 doi:10.20944/preprints202506.0719.v1

sample. Finally, its effective refractive index and corresponding concentration are determined using reflectance (resonance angle, depth) and the van de Hulst formula (real part and imaginary part of effective refractive index).

2. Theory

In physics, chemistry, and biology, surface plasmon resonance (SPR), and coherent scattering theory (CST) have gained significant importance in the research of diverse topics, including the study of colloids and suspensions (fluids containing nanoparticles and microparticles, respectively), as they allow us to understand the iterations of light with samples [3,4,17,22,23]. Figure 1 shows a sensor with a coherent light source, a polarizer (P), a photodiode, a semicircular prism, a metallic thin film (TF), and particles in a dielectric medium to illustrate the phenomena of SPR and coherent scattering.

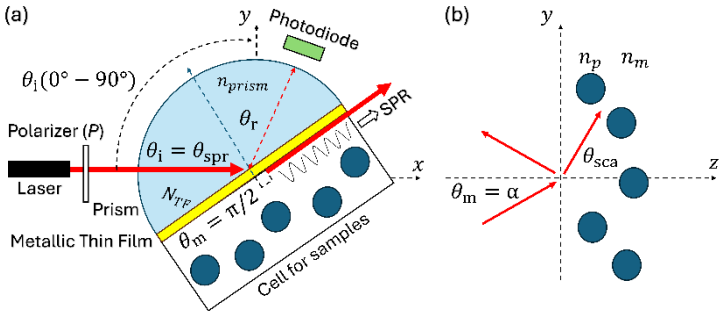

Figure 1. (a) Sensor, with Kretschmann-Raether configuration, for the detection of particles in a colloid or suspension, and (b) reflection and transmission of coherent light in a dielectric medium with particles. .

A film is considered thin when all interference effects in reflected or transmitted coherent light can be detected. Interference effects depend on the illumination source and the thickness and refractive index (RI) of each layer, where each layer is represented by a 2x2 matrix. In normal coatings, the films (metals and dielectrics) will be thin, while the substrates will be thick. The reflectance, admittance, and the characteristic matrix, of an assembly of thin films for oblique incidence in absorbing media, are expressed respectively as [28]:

$$R = |r|^2 = \left|\frac{\eta_0 - Y}{\eta_0 + Y}\right|^2 \tag{1}$$

$$Y = \frac{H}{E} \tag{2}$$

$$\begin{bmatrix} E \\ H \end{bmatrix} = \prod_{j=1}^{q} \begin{bmatrix} \cos\delta_j & -(i\sin\delta_j)/\eta_j \\ -(i\sin\delta_j)\eta_j & \cos\delta_j \end{bmatrix} \begin{bmatrix} 1 \\ \eta_{q+1} \end{bmatrix} \tag{3}$$

where r is the reflection coefficient, η_0 is the tilted admittance on the incident medium, η_{q+1} is the tilted admittance of the substrate or emergent medium, Y is the optical admittance of the multilayer system, H and E represent the amplitude of the magnetic and electric fields, respectively. $\delta_j = (2\pi/\lambda_0)d_j N_j \cos\theta_j$ is the phase thickness, λ_0 is the wavelength, d is the physical thickness, $N = (n + ik)$ is the complex refractive index, θ is the angle of incidence, j is the layer number from 1 to q, $N_j \cos\theta_j = \left[N_j^2 - (n_0 \sin\theta_0)^2\right]^{1/2}$, for s- polarization $\eta_{j(s)} = \mathcal{Y}\left[N_j^2 - (n_0 \sin\theta_0)^2\right]^{1/2}$, for p-polarization $\eta_{j(p)} = \mathcal{Y}N_j^2/\left[N_j^2 - (n_0 \sin\theta_0)^2\right]^{1/2}$, and $\mathcal{Y}$ the optical admittance in free space equal to 2.6544×10^{-3} Siemens.

SPR was developed over time by several researchers[18–21] . In SPR, surface plasmon excitation occurs at the interface of a metallic thin film and a dielectric medium, when a coherent light source undergoes total internal reflection. The coherent light beam then excites the surface electrons of the metallic film, causing them to interact with the dielectric medium containing the sample

 doi:10.20944/preprints202506.0719.v1

(biomolecules, analytes, or particles). The SPR technique allows the detection of very small changes in the refractive index of a metallic surface (which has surface plasmons, or collective electron oscillations) when the molecules or particles in the sample bind to the metal surface while scattering (plasmonic scattering) detects the light scattered by these molecules/particles at the surface.

From CST researchers, two formulas are presented here to calculate the effective refractive index. Equation (4) for a dilute monodisperse system of randomly located spherical particles, developed by García-Valenzuela et. al [24,25], and equation (5) for a monodisperse system (isotropic and independent of polarization) of spherical particles, developed by H.C. van de Hulst [26]:

$$\tilde{n}_{eff} = n_m \left[1 + 2i \left(\frac{2\pi\rho}{k_m^3} \right) S_0 - \left(\frac{2\pi\rho}{k_m^3} \right)^2 \frac{\left(S_0^2 - S_j^2 \right)}{cos^2\theta_m} \right]^{1/2} \quad (4)$$

$$\tilde{n}_{eff} = n_m \left[1 + i \left(\frac{2\pi\rho}{k_m^3} \right) S_0 \right] \quad (5)$$

where n_m is the refractive index of the medium surrounding the particles, i is the imaginary unit ($\sqrt{-1}$), ρ is the number concentration of the particles, $k_m = 2\pi/\lambda$ is the wavenumber of the incident wave in the medium, and the functions $S_j = S_j(N, x, u = \cos\theta_{sca})$ that can be S_0, S_1 or S_2, S_0 ($\theta_{sca} = 0$) is the forward-scattering amplitude, S_1 for s-polarization (TE: Transverse Electric) and S_2 for p-polarization (TM: Transverse Magnetic) are the components of the amplitude scattering matrix, calculated by Mie scattering theory [23]. θ_m , which has the form $\pi/2 + |\alpha i|$ [3], is the angle of incidence in the dielectric medium for the evanescent field, and $\theta_{sca} = \pi - 2\theta_m$ [24,25] is the scattering angle. θ_m can be calculated from the resonance angle θ_{spr} by sequentially applying Snell's law at the interfaces (Prism – Thin film of gold – Matrix material, dielectric medium, colloid, or suspension) [3,24,25]. Also $N = n_p/n_m$ is the relative refractive index, $x = k_m a$ is the size parameter, λ_o is the wavelength in vacuum, $\lambda = \lambda_o/n_m$ is the wavelength of the incident light in the surrounding medium, n_p is the refractive index of a spherical particle, a is the radius of the spherical particle, $f = \rho V$ is the particle fill fraction, and $V = (4/3)\pi a^3$ is the volume of a spherical particle.

In CST [22], the study of incident coherent light and coherent light scattered in a certain direction, passing through spherical particles of any size and material immersed in a surrounding medium (transparent, homogeneous, and isotropic), is described with formulas that are exact solutions to Maxwell's equations, which were developed by Gustav Mie [23]. Light scattering is the phenomenon where light is redirected by an object. The scattered wave is composed of several partial waves, whose amplitudes depend on a_m (mth electric partial wave), b_m (mth magnetic partial wave), π_m and τ_m:

$$S_1 = \sum_{m=1}^{\infty} \frac{2m+1}{m(m+1)} [a_m \pi_m(u) + b_m \tau_m(u)] \quad (6)$$

$$S_2 = \sum_{m=1}^{\infty} \frac{2m+1}{m(m+1)} [b_m \pi_m(u) + a_m \tau_m(u)] \quad (7)$$

$$a_m(N, x, z) = \frac{N\, \psi_m(z)\, \psi_m'(x) - \psi_m(x)\, \psi_m'(z)}{N\, \psi_m(z)\, \xi_m'(x) - \xi_m(x)\, \psi_m'(z)} \quad (8)$$

$$b_m(N, x, z) = \frac{\psi_m(z)\, \psi_m'(x) - N\, \psi_m(x)\, \psi_m'(z)}{\psi_m(z)\, \xi_m'(x) - N\, \xi_m(x)\, \psi_m'(z)} \quad (9)$$

$$\psi_m(\sigma) = \sqrt{\pi\sigma/2}\, J_{m+1/2}(\sigma) \quad (10)$$

$$\varphi_m(\sigma) = \sqrt{\pi\sigma/2}\, J_{-m-1/2}(\sigma) \cdot (-1)^m \quad (11)$$

$$\xi_m(\sigma) = \psi_m(\sigma) + i\varphi_m(\sigma) \quad (12)$$

$$\pi_m(u) = \frac{\partial P_m(u)}{\partial u}; \quad \pi_m'(u) = \frac{\partial^2 P_m(u)}{\partial u^2} \quad (13)$$

$$\tau_m(u) = u\, \pi_m(u) - (1 - u^2)\pi_m'(u) \quad (14)$$

 doi:10.20944/preprints202506.0719.v1

where a_m and b_m are the amplitude functions, $\pi_m(u)$ and $\tau_m(u)$ are the angular functions, $m = 1, \ldots, m_{max}$ is the number of terms in the summation, $m_{max} = round(4x^3 + x + 2)$ is the maximum number rounded to the nearest integer, $\psi'_m(\sigma)$ and $\xi'_m(\sigma)$ are the partial derivatives of $\psi_m(\sigma)$ and $\xi_m(\sigma)$ respectively, the argument σ takes on the values x or $z = Nx$, $J_{m+1/2}(u)$ and $J_{-m-1/2}(u)$ are the Bessel functions of positive and negative half-order, respectively. The angular functions π_m and τ_m containing the scattering angle θ_{sca}, P_m is the Legendre polynomial of degree m, and $u = \cos\theta_{sca}$.

In this work, with an optomechatronic system and applications that we have developed, the processing of the signals for SPR and CTS is carried out in real-time and post-processing for the analysis of the signals, from the measurement of the thin film deposited on the prism to the detection of spherical polystyrene particles in a solution and the calculation of effective refractive index.

3. System and Methodology

The Optomechatronic System [27] is formed of a laser diode with a wavelength of $\lambda_0 = 639$ nm (Mod. LPM690-30C, Newport Corporation, Irvine, California, USA), a linear polarizer P (Mod. 5511 General Purpose Sheet Polarizer, 450-750 nm, Newport Corporation, Irvine, California, USA), a semicircular prism (FK5, n=1.4585 [29]) with gold metallic thin film (Purity of 99.99%, Kurt J. Lesker Co., Clairton, PA, USA) and glass cell to colloids or suspension samples (5 μm diameter SPSP, Number 02705-AB, SPI Supplies, West Chester, Pennsylvania, USA), a silicon photodiode (Mod. S1226-8BK, Hamamatsu Photonics K.K., Hamamatsu City, Japan), two motorized rotation stages (Mod. 8MR180-2, Standa LTD, Lithuania), a cabinet with power and control electronics, control program (LabVIEW, Version 2020, National Instruments, Ciudad Juárez, México), simulation and post-processing program (MATLAB, Version 2024, MathWorks, Inc., Massachusetts, USA), ana personal computer (Windows 10, Intel Core i7, 2.6 GHz, 12 GB RAM, 1 TB SSD).

According to the concentration and volume formula for dilutions ($C_iV_i = C_fV_f$), for an initial concentration of 1% of SPSP in distilled water and a final volume of 3000 μL, by adding an initial volume of 0, 60, 150, 1500, and 3000 μL, a final concentration percentage of 0.00, 0.20, 0.05, 0.50 and 1.00 % of PS in distilled water can be obtained.

Once the samples are obtained, the system is adjusted with the laser and prism at 0 and 90 degrees. Each homogenized sample of the PS solution is placed in the prism cell, and an angular scan of 30 to 80 degrees is performed to obtain the reflectance signal with SPR-Scattering.

The reflectance (Eq. 1-3) of the sensor (Figure 1) with SPR-Scattering can be simulated (Figure 2a-b, signal in black) when the coherent light ($\lambda_0 = 639\,nm$) is p-polarized, the gold thin film ($N_{Au} = 0.1736 + 3.4930i$ [30], the thickness of 51 nm) in the prism ($n_{prism:\,FK5} = 1.4858$) adjoins a dielectric medium (for example, distilled water with $n_m = 1.3314$ [30]), and there is a total internal reflection ($n_{prism} > n_m$). From the reflectance, the resonance angle $\theta_{spr} = 75.11°$ is obtained, which is used to obtain the angle of incidence in the medium $\theta_m = \pi/2 + |-0.393673|$i using Snell's law, and the scattering angle $\theta_{sca} = \pi - 2\theta_m$.

Then, to calculate the effective refractive index (Eq. 4, 6-14) for spherical (radius $a = 25\,nm$) polystyrene ($n_p = 1.5870$ [30]) particles in distilled water with a concentration of $f = 0.02$ %, it is necessary to calculate S_0 ($1.2125\times 10^{-5} - 4.3613\times 10^{-3}i$), S_1 ($1.2126\times 10^{-5} - 4.3934\times 10^{-3}i$) and S_2 ($1.6082\times 10^{-5} - 5.8211\times 10^{-3}i$) for the corresponding relative refractive index $N = n_p/n_m = 1.1920$, the wavenumber of the incident wave in the medium $k_m = 1.30914443\times 10^7 m^{-1}$, the size parameter $x = 0.3273$, $z = Nx = 0.3901$; number of terms in the summation $m_{max} = 5$, $\theta_m = \pi/2 + 0.3937i$, and $\theta_{sca} = -0.7873i$, where $\psi_1(w) = sin(w)/w - cos(w)$; $\varphi_1(w) = -cos(w)/w - sin(w)$; $\pi_1(w) = 1$, and $\tau_1(w) = w$ for $w = \cos(\theta_{sca})$, $a_1 = 8.0816\times 10^{-6} - 2.8428\times 10^{-3}i$ and $b_1 = 1.2067\times 10^{-9} - 3.4738\times 10^{-5}i$. The result of the calculation is $\tilde{n}_{eff} = 1.331450 + 1.381626\times 10^{-7}i$, which is simulated as a medium in reflectance (Eq. 1), is graphed in Figure 2a-b (red signal). The same procedure is performed for concentrations of 0.05, 0.50, and 1.00 % (Figure 2a-b, signals in green, cyan, and magenta, respectively).

 doi:10.20944/preprints202506.0719.v1

For particles with radii greater than 850 nm, Eq. (4) takes values greater than n_p and then values that grow exponentially, so Eq. (5) or Eq. (15) can be used to calculate the $\tilde{n}_{eff}$ of 5 μm diameter or 2.5 μm radius SPSP in distilled water with different concentrations. Table 1 shows the effective refractive indices calculated for SPSP of 25 nm and 2.5 μm radius, using Eq. (4) and Eq. (5) or (15), respectively.

$$\tilde{n}_{eff} = n_m \left[1 + i\frac{3}{16}\left(\frac{\lambda_o}{\pi\, n_m}\right)^3 \frac{f}{a^3} S(n_p/n_m, 2\pi n_m a/\lambda_o, u = 1)\right] \qquad (15)$$

As can be seen in Figure 2a-b and Table 1, for nanoparticles, the resonance angle shifts to the right as particle concentration increases, and their refractive index can be differentiated from the fifth digit. Whereas in Figure 2c-d and Table 1, for microparticles, the reflectance has almost the same resonance angle and the depth tends to be smaller as particle concentration increases, and the refractive index can be differentiated from the sixth digit.

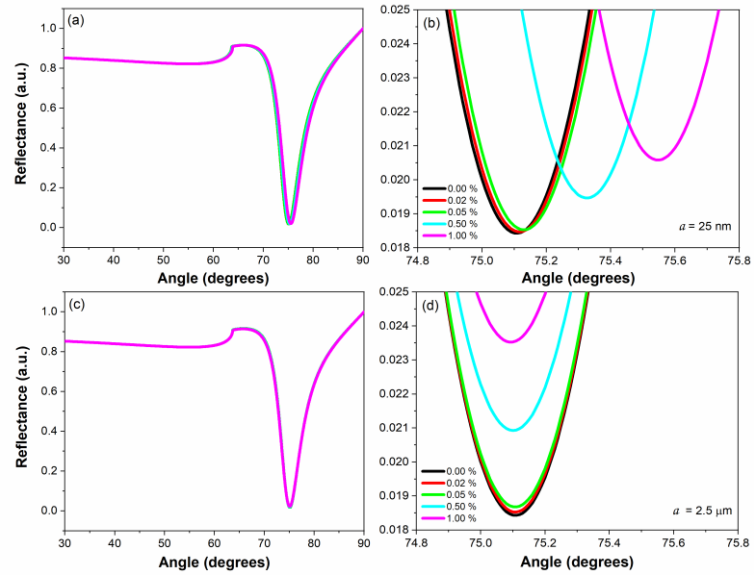

Figure 2. Simulation of reflectance for a solution containing SPSP of 25 nm (a-b) and 2.5 μm (c-d) of radius, with concentrations of 0.00, 0.02, 0.05, 0.50, and 1.00 % in distilled water. The prism is an FK5, which has a thin film of gold (51 nm of thickness) and a cell for the sample of colloid or solution.

Table 1. Theoretical effective refractive indices for spherical polystyrene particles with a radius of 25 nm and 2.5 μm with concentrations of 0.00, 0.02, 0.05, 0.50, and 1.00% immersed in distilled water.

	$\tilde{n}_{eff}$ (Eq. 4) $a = 25\ nm$		$\tilde{n}_{eff}$ (Eq. 5 or Eq. 15) $a = 2.5\ \mu m$	
% PS	n	k	n	k
0.00	1.331400	0	1.331400	0
0.02	1.331450	1.3816E-7	1.331398	6.5749E-6
0.05	1.331524	3.4548E-7	1.331396	1.6437E-5
0.50	1.332644	3.4656E-6	1.331360	1.6437E-4
1.00	1.333893	6.9550E-6	1.331320	3.2874E-4

Figure 3 a-b shows the real and imaginary parts of the effective refractive index for different solutions with spherical particles of 0.5 μm, 2.5 μm, 5 μm, and 7.5 μm radius in distilled water, with concentrations of 0-1%. Figures 3 c-f show the respective reflectances, where the reflectance depth

 doi:10.20944/preprints202506.0719.v1

values for spherical particles with a radius of 7.5 μm (Figure 3f) are within the reflectance of the 5 μm ones (Figure 3e), the 5 μm reflectance depth values are within the reflectance of the 2.5 μm ones (Figure 3d), and the 2.5 μm values are within the reflectance of 0.5 μm (Figure 3c). Therefore, with the angular scanning technique in SPR, the size of the particles can only be differentiated from 1% of the filling fraction, if the diameter or radius of the particle is not known as a priori.

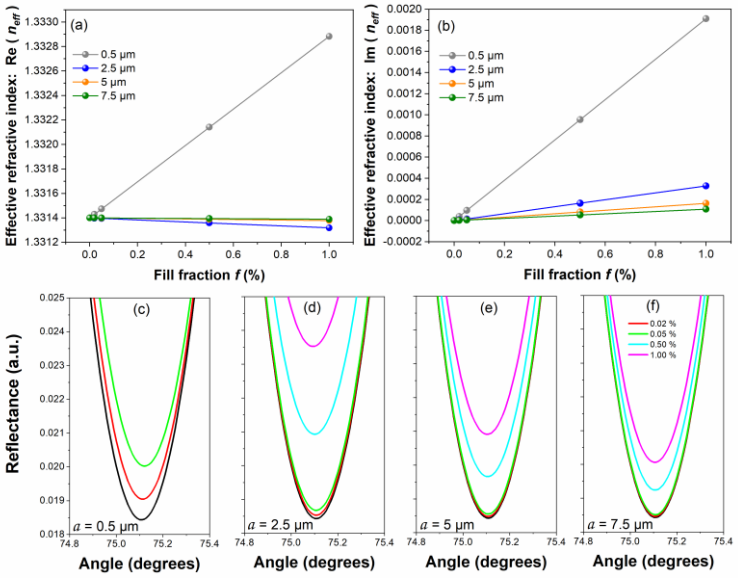

Figure 3. Simulation of scattering and SPR. (a) refractive index, (b) extinction coefficient, and (c-f) respective reflectances, for solutions with spherical particles of 0.5 μm, 2.5 μm, 5 μm, and 7.5 μm radius in distilled water.

From Eq. (15), the real and imaginary parts of the effective refractive index will be given by:

$$\tilde{n} = n_m - n_m C_1 \frac{f}{a^3} Im\left[S(n_p/n_m, 2\pi n_m a/\lambda_o, u = 1)\right] \qquad (15b)$$

$$\tilde{k} = n_m C_1 \frac{f}{a^3} Re\left[S(n_p/n_m, 2\pi n_m a/\lambda_o, u = 1)\right] \qquad (15c)$$

where C_1 is equal to $(3/16)\left(\lambda_o/(\pi n_m)\right)^3 = 6.6854 \times 10^{-22}$ if $n_m = 1.3314$ and $\lambda_o = 639\, nm$.

Knowing the refractive index of the prism (n_{prism}), the metallic film (N_{Au}) and its thickness (51 nm), and the water (n_m) as the base sample, we have an initial reference point $(75.11°, 0.0184)$ for $f = 0\%$: $\tilde{n} = n_m$ and $\tilde{k} = 0$. Thus, the real part will be affected by changes in the resonance angle and the imaginary part by the depth of the reflectance. As mentioned above, different mathematical methods have already been demonstrated to know the three main parameters (a, f, n_p), so in this situation we are only going to measure the concentration knowing a priori the refractive index ($n_p = 1.5870$) and the radius ($a = 2.5\, \mu m$) of the spherical particle. For the deeper points of the signals (Figure 2d and 3d), the effective refractive index (sample in the dielectric medium) can be calculated by giving values to f in equations 15 b-c until they coincide with the minimum value of its reflectance.

In this way, the methodology consists of obtaining the theoretical value of the effective refractive index ($\tilde{n}_{eff}$) for each concentration of the colloid or solution sample, substitute it in the reflectance formula as the dielectric medium, and graph the expected theoretical SPR-Scattering signal. The experimental air reflectance is then fitted to the theoretical signal (simulated) to determine the thickness of the gold film deposited on the flat face of the semicircular prism. Finally, the experimental reflectance of the distilled water is adjusted to the simulated one, to know the displacements (degrees), amplitudes (reflectance), and losses or gains, which must be applied to all the experimental signals to find their respective effective refractive index and concentration using Eq. 15 b-c.

 doi:10.20944/preprints202506.0719.v1

4. Results and Discussion

Suspensions must be homogenized before use, they must not be frozen or shaken vigorously, at least ten particles must be measured in image visualization, store at room temperature with the bottle tightly covered, and in case of spillage, be sure to rinse with plenty of water and dispose of it as normal laboratory waste. To ensure a homogeneous suspension of samples with 5 μm diameter or 2.5 radius SPSP (manufactured by SPI Supplies), the bottle was gently inverted several times until no sediment or clumps were observed. It was then immersed in an ultrasonic water bath (C008 40 KHz, AcmeSonic Ltd., Shenzhen, China) for one minute at low power. The desired sample was immediately withdrawn from the bottle using a pipette (Ecopipette 20-200 & 100-1000 μL, CAPP AHN Biotechnologie GmbH, Nordhausen, Germany). The concentration of SPSP was 0.00, 0.02, 0.05, 0.50, and 1.00 % in distilled water.

Figure 4 (a) shows the adjustment of the experimental air sample with the theoretical signal to determine the thickness of the thin gold film deposited on the flat face of the prism, resulting in a 51 nm thin gold film. Figure 4 (b) shows the adjustment of the reflectance of the distilled water sample to the theoretical signal with a reference point at 75.11°, 0.0184 depth. The displacement, amplitude, and gain/loss parameters used in the adjustment are subsequently applied to all samples, resulting in Figure 4 (c).

To calculate $\tilde{n}_{eff}$ and f from the magenta signal shown in Figure 4c with its resonance angle and depth of 75.09° and 0.0234, respectively, with relative refractive index ($N = n_p/n_m$=1.1920), particle size ($x = 2\pi n_m a/\lambda_o$=32.7286), and forward scattering $S_0 = 577.0855 + 141.0735i$, the value of f is introduced in equations (15b) and (15c), from 0.00 with increments of 0.01, until the value of $\tilde{n}+\tilde{k}$ introduced in the external medium of thin films gives us the value of the angle of resonance and the depth of the reflectance. So, in this case (magenta signal of Figure 4c), the effective refractive index is $\tilde{n}_{eff} = 1.331322 + 3.1888 \times 10^{-4} i$ for a concentration of 0.97 %. The effective refractive indices and their concentrations obtained for the reflectances in Figure 4c are shown in Table 2, where the smallest error was 0.03 % ($f = 0.02, 0.50$, and 1.00 %).

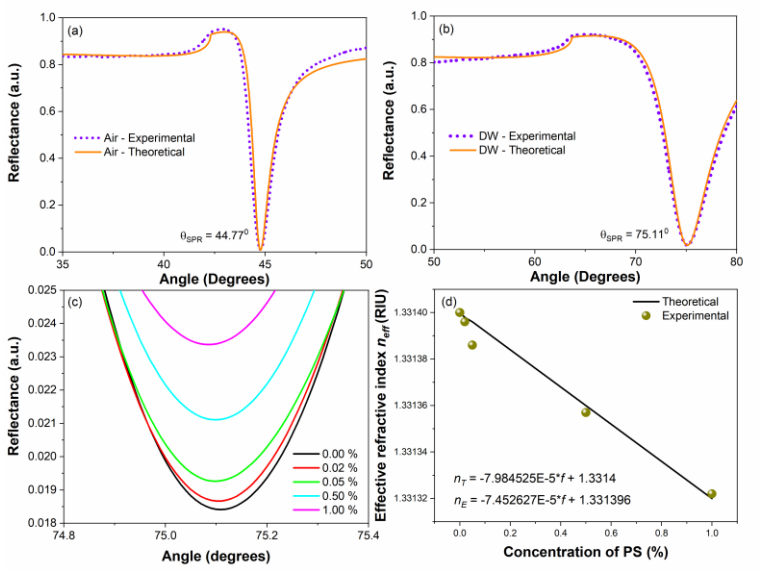

Figure 4. (a) Fitting of the experimental reflectance of air to the theoretical signal, (b) fitting of the experimental reflectance of distilled water to the theoretical signal, (c) SPR-Scattering reflectance signals for different percentages of PS in distilled water, and (d) theoretical calculation and experimental measurement for different concentrations.

Table 2. Experimental effective refractive indices for SPSP in distilled water. The spherical PS particles have a 5 μm diameter or 2.5 radius, a refractive index of $n_p = 1.5870$, and different concentrations (%).

 doi:10.20944/preprints202506.0719.v1

$\tilde{n}_{eff}$ (Eq. 15b and Eq. 15c) $a = 2.5\ \mu m$		
% PS	n	k
0.00	1.331400	0
0.05	1.331396	1.6437E-5
0.17	1.331386	5.5856E-5
0.53	1.331357	1.7423E-4
0.97	1.331322	3.1888E-4

The optoelectronic system has a resolution of 0.01 degrees and a precision of 0.0071 RIU (Refractive Index Unit). For very small concentrations (0.00, 0.02, 0.05, 0.50, and 1.00 %) of 2.5 μm radii SPSP in distilled water, the experiment provides a good linear fitting of R^2=0.986, a sensitivity of -7.4526 $\times 10^{-5}$ RIU/% (Figure 4d), LOD=0.001% and LOQ=0.0035%. It is very important to correctly determine the thickness of the thin gold film (51 nm), since it determines the measurement range in the reflectance amplitude, equal to 0.0051 nm, where the concentrations and the extinction coefficient are mainly measured since n is approximately equal to 1.3314 for all solutions. To avoid potential errors when the laser power varies, a beam splitter and a photodiode were added to the portable optoelectronic system to provide reference power.

After each test, it is recommended to recover the sample by subtracting the solution with the corresponding or labeled syringe for each sample, then clean the cell with methanol by introducing it into its corresponding syringe and leaving it for 1 minute, finally rinsing about 5 times with distilled water.

A sample of 5 μm diameter or 2.5 radius SPSP suspension was taken from the manufacturer's bottle and allowed to dry on a slide for microscopic observation (Figure 5). The diameter measurements (4.6; 4.2; 3.8; 4.6; 4.7; 5.1; 4.9; 5.5; 5.3; and 5.2) yielded an average of 4.76 μm and a standard deviation of 0.45 μm.

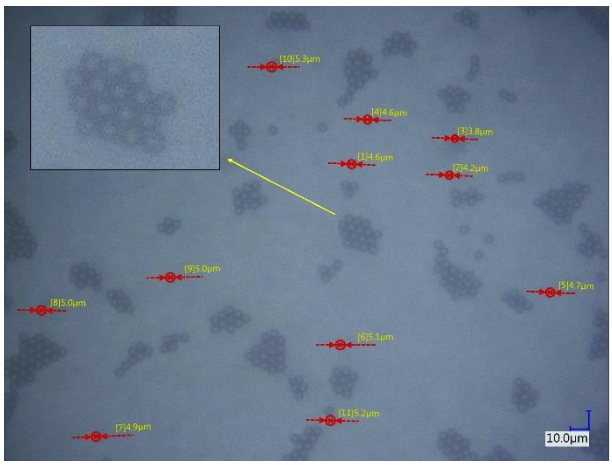

Figure 5. Polystyrene microspheres of 5 μm μm diameter or 2.5 radius SPSP viewed with a digital microscope (VHX-5000, Keyence Corporation, Osaka, Japan).

Figure 6 shows two main functions of the application developed in MATLAB for our portable optomechatronic system. The reflectance function with SPR (Figure 6a) is used to simulate a semicircular prism with 1-6 thin films and a dielectric medium at a given wavelength and to fit an experimental signal to a simulated theoretical signal. The reflectance function with Mie Scattering (Figure 6b) is used to simulate a semicircular prism with 1-2 thin films and a dielectric medium at a given wavelength and to calculate the effective refractive index (Eq. 4 or 5) using Mie scattering theory.

 doi:10.20944/preprints202506.0719.v1

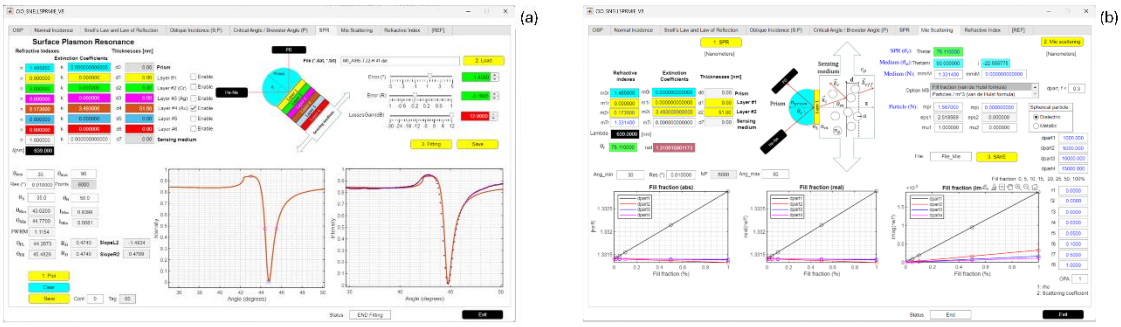

Figure 6. Application developed in MATLAB to process the theoretical and experimental signals of (a) SPR and (b) Scattering.

For the simulation of SPR curves based on the Fresnel formalism, there is the free software WinSpall 3.01 [31]. There are also tables [32–34], MATLAB functions [35], calculator [36], and software [37] that can help us verify, obtain, or display, the Mie theory's scattering functions for spherical particles.

5. Conclusion

In this work, we present a methodology for measuring the effective refractive index and concentration for a solution containing 5 μm diameter or 2.5 radius spherical polystyrene particles. We analyze the reflectance signals, their resonance angles, and depths, which are affected by SPR and scattering. This paper presents the mathematical tools used for SPR and Scattering; the functionality of the portable optomechatronic system; and the control and simulation applications developed. The methodology includes measuring the thickness of the thin gold film (51 nm), which is very important because it determines the depth measurement range (0.0051 nm) for the concentrations used (0.00, 0.02, 0.05, 0.50, and 1.00%). The measurement error for concentrations of 0.02%, 0.50% and 1.00% was 0.03%. Possible sources of error in colloid and solution measurement are the degree resolution of the system and the stability of the laser.

Funding: The authors want to thank the Secretaría de Ciencia, Humanidades, Tecnología e Innovación (SECIHTI) for funding through the program Estancias Postdoctorales por México, CVU 740156 and CVU 101368.

Data Availability Statement: The data generated and analyzed during the current study are available from the corresponding author.

Disclosures: The authors declare no conflicts of interest.

References

1. Frias JPGL, Nash R. Microplastics: Finding a consensus on the definition. Mar Pollut Bull 2019;138:145–7.
2. Gigault J, Ter Halle A, Baudrimont M, Pascal PY, Gauffre F, Phi TL, et al. Current opinion: what is a nanoplastic? Environmental Pollution 2018;235:1030–4.
3. Tuoriniemi J, Moreira B, Safina G. Determining number concentrations and diameters of polystyrene particles by measuring the effective refractive index of colloids using surface plasmon resonance. Langmuir 2016;32:10632–40.
4. Márquez-Islas R, Sánchez-Pérez C, García-Valenzuela A. Determination of refractive index, size, and concentration of nonabsorbing colloidal nanoparticles from measurements of the complex effective refractive index. Opt Lett 2014;39:559–62.
5. Thompson RC, Olsen Y, Mitchell RP, Davis A, Rowland SJ, John AWG, et al. Lost at sea: where is all the plastic? Science (1979) 2004;304:838.

 doi:10.20944/preprints202506.0719.v1

6. Thompson RC, Courtene-Jones W, Boucher J, Pahl S, Raubenheimer K, Koelmans AA. Twenty years of microplastic pollution research—what have we learned? Science (1979) 2024;386:eadl2746.
7. Adediran GA, Cox R, Jürgens MD, Morel E, Cross R, Carter H, et al. Fate and behaviour of Microplastics (> 25μm) within the water distribution network, from water treatment works to service reservoirs and customer taps. Water Res 2024;255:121508.
8. Ya H, Jiang B, Xing Y, Zhang T, Lv M, Wang X. Recent advances on ecological effects of microplastics on soil environment. Science of the Total Environment 2021;798:149338.
9. Issac MN, Kandasubramanian B. Effect of microplastics in water and aquatic systems. Environmental Science and Pollution Research 2021;28:19544–62.
10. Vo HC, Pham MH. Ecotoxicological effects of microplastics on aquatic organisms: a review. Environmental Science and Pollution Research 2021;28:44716–25.
11. Leonard SVL, Liddle CR, Atherall CA, Chapman E, Watkins M, Calaminus SDJ, et al. Microplastics in human blood: Polymer types, concentrations and characterisation using μFTIR. Environ Int 2024;188:108751.
12. Kwon JH, Kim JW, Pham TD, Tarafdar A, Hong S, Chun SH, et al. Microplastics in food: a review on analytical methods and challenges. Int J Environ Res Public Health 2020;17:6710.
13. Sapkale D, Kurkute P, Mistry A, Pandit S V. Polyethylene Microplastics Affected Survival Rate, Food Intake and Altered Oxidative Stress Parameters in Freshwater Snail Indoplanorbis exustus. Bull Environ Contam Toxicol 2023;111:67.
14. Berber AA. Genotoxic evaluation of polystyrene microplastic. Sakarya University Journal of Science 2019;23:358–67.
15. Primpke S, Wirth M, Lorenz C, Gerdts G. Reference database design for the automated analysis of microplastic samples based on Fourier transform infrared (FTIR) spectroscopy. Anal Bioanal Chem 2018;410:5131–41.
16. Ragusa A, Notarstefano V, Svelato A, Belloni A, Gioacchini G, Blondeel C, et al. Raman microspectroscopy detection and characterisation of microplastics in human breastmilk. Polymers (Basel) 2022;14:2700.
17. Luna-Moreno D, Sánchez-Espinosa YM, Ponce de León YR, Arias EN, Garnica-Campos G. Virtual instrumentation in LabVIEW for multiple optical characterizations on the same opto-mechanical system. Optik-International Journal for Light and Electron Optics 2015;126:1923–9.
18. Pines D, Bohm D. A collective description of electron interactions: II. Collective vs individual particle aspects of the interactions. Physical Review 1952;85:338.
19. Otto A. Excitation of nonradiative surface plasma waves in silver by the method of frustrated total reflection. Zeitschrift Für Physik A Hadrons and Nuclei 1968;216:398–410.
20. Kretschmann E. Die bestimmung optischer konstanten von metallen durch anregung von oberflächenplasmaschwingungen. Zeitschrift Fur Physik 1971;241:313–24.
21. Liedberg B, Nylander C, Lunström I. Surface plasmon resonance for gas detection and biosensing. Sensors and Actuators 1983;4:299–304.
22. Bohren CF, Huffman DR. Absorption and scattering of light by small particles. John Wiley & Sons; 2008.
23. Gustav M. Beitraege zur Optik trueber Medien. Ann Physik 1908;25:377.
24. Barrera RG, Garcıa-Valenzuela A. Coherent reflectance in a system of random Mie scatterers and its relation to the effective-medium approach. Journal of the Optical Society of America A 2003;20:296–311.
25. García-Valenzuela A, Barrera RG, Sánchez-Pérez C, Reyes-Coronado A, Méndez ER. Coherent reflection of light from a turbid suspension of particles in an internal-reflection configuration: Theory versus experiment. Opt Express 2005;13:6723–37.

 doi:10.20944/preprints202506.0719.v1

26. H. C. van de Hulst. Light scattering by small particles. Quarterly Journal of the Royal Meteorological Society 1958;84:198–9.
27. Sánchez-Alvarez A, Rodríguez-Quiroz O, Quintanilla-Villanueva GE, Rodríguez-Delgado MM, Villarreal-Chiu JF, Silva-Hernández OJ, et al. Development of a Portable Optomechatronic System to Obtain the Characterization of Transparent Materials and Dielectric Thin Films. Optics 2024;5:595–610.
28. Macleod HA. Thin-film optical filters. Thin-Film Optical Filters, Fourth Edition 2010:1–782.
29. Available online: SCHOTT 2025. https://www.schott.com/pt-br/special-selection-tools/interactive-abbe-diagram (accessed May 27, 2025).
30. Available online: Refractive Index 2025. https://refractiveindex.info/?shelf=main&book=H2O&page=Hale (accessed January 27, 2025).
31. Available online: Res-Tec-DE 2025. http://www.res-tec.de/downloads.html (accessed May 27, 2025).
32. Lowan A. Tables of Scattering Functions for Spherical Particles. Applied Math Series 4 (US Nat Bur Stand, Washington) 1948.
33. Gumprecht RO, Sliepcevich CM. Tables of light-scattering functions for spherical particles. Eng Res Inst, Univ of Michigan 1951.
34. Goldberg B. New Computation of the Mie Scattering Functions for Spherical Particles. J Opt Soc Am 1953;43:1221_1-1222.
35. Matzler C. MATLAB functions for Mie scattering and absorption. 2002.
36. Available online: Mie Scattering Calculator 2025. https://omlc.org/calc/mie_calc.html (accessed May 27, 2025).
37. Ma D, Tuersun P, Cheng L, Zheng Y, Abulaiti R. PyMieLab_V1.0: A software for calculating the light scattering and absorption of spherical particles. Heliyon 2022;8:e11469.